IOP Publishing Smart Materials and Structures
Smart Mater. Struct. **28** (2019) 075002 (8pp) https://doi.org/10.1088/1361-665X/ab1ab3

Design and characterization of electrostatic zipper hinges

Marcos B Oliveira, Colin B Davis, Samuel C Bradford, Thomas P Disarro, James A Smith and Samuel M Felton

Department of Mechanical and Industrial Engineering, Northeastern University, 360 Huntington Avenue, Boston, MA 02115, United States of America

E-mail: s.felton@northeastern.edu

Received 7 November 2018, revised 15 April 2019
Accepted for publication 18 April 2019
Published 20 May 2019

Abstract

In this paper we present the design and characterization of actuated hinges based on the electrostatic zipper architecture. We compare three designs that integrate the zipper actuator with a flexural hinge and mechanical transmission. For each design, we present a model to predict displacement and validate it experimentally, characterizing its step response, torque, and repeatability. The results indicate that electrostatic zipper hinges are substantially faster than alternative self-folding actuators. They can be designed to produce large fold angles (over 100°) and repeatable analog behavior. These results suggest that this actuator can be applied to self-adjusting origami solar arrays and high-speed self-folding structures.

Keywords: actuators, electrostatics, self-folding, origami

(Some figures may appear in colour only in the online journal)

1. Introduction

Origami engineering is an effective paradigm for a variety of engineering systems including microscale fabrication [1, 2], mechanically tunable structures [3, 4], and transformable robotics [5–7]. Particularly relevant to this paper, space engineering has used origami concepts to transport and deploy satellites [8, 9]. Some of these systems actuate themselves along the fold lines in a process known as self-folding. This is typically accomplished by low-profile actuators installed at rotary hinges, and has been implemented with shape memory alloys [10], shape memory polymers [11], swelling hydrogels [12], and pneumatics [13], among other methods. Self-folding has been applied to make structures and machines from the meter [13] to the micrometer [14] scale with a variety of performance characteristics and functionalities. However, many of these techniques share certain critical limitations: the majority of methods are slow, irreversible, and difficult to control. For example, open-loop actuation of shape memory composites results in deviations of 5°–8° between hinges, and these are mechanically pre-programmed, so they can only target a single reference angle [15, 16].

One application where self-folding could be valuable is in the controlled actuation of self-adjusting solar arrays [17, 18]. Origami-inspired arrays consist of multiple plates connected by discrete hinges [9] and in order to optimize their power collection, the plates must maintain a precise alignment relative to the Sun. If the hinges connecting these plates were actuated, they could correct for deviations caused by drift, thermal expansion, or imperfect deployments. However, to accomplish this, the actuators would need to be fast, precise, and low-power.

To address this need, we have developed and characterized a new self-folding actuator that uses an electrostatic zipper architecture to drive a rotary joint in a low-profile form (figure 1). We show that this approach to self-folding is fast and repeatable. We present three possible designs along with models and experimental data validating their performance.

2. Background

2.1. Electrostatic actuators

Electrostatic actuators are driven by the attractive force between two electrodes with opposite charges, governed by Coulomb's Law. They are often used for adhesion [19] or actuation of microscale structures [20]. If we consider a

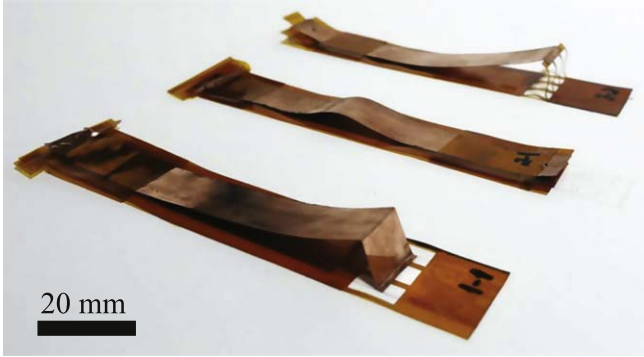

Figure 1. This paper presents the design and characterization of three actuated hinges driven by electrostatic zippers.

parallel plate capacitor with plate area A, gap width d, gap dielectric permittivity ϵ and a voltage potential V, we can model the attractive force between them as proportional to the square of the voltage and inversely proportional to the square of the distance.

$$F_{att} = \frac{\epsilon A V^2}{2d^2}. \quad (1)$$

Electrostatic actuators are often used in parallel with a linear elastic spring to provide a restoring force. Because the electrostatic force is quadratically related to the plate displacement and the spring force is linearly related to the plate displacement, there is generally a plate separation distance where the system reaches an instability and the plates snap together. This transition from analog to bistable behavior is referred to as 'pull-in'. For parallel plate capacitors with a linear spring, the pull-in point is approximately $1/3$ of the original gap length [21]. While some actuators use the bistable behavior, others can only operate within the analog regime. Because of this, various designs have been implemented to expand this analog range.

2.2. Electrostatic zipper actuators

The electrostatic zipper is a specific type of electrostatic actuator that can achieve relatively large displacements [22–24]. It takes the parallel plate actuator concept but tilts the top electrode so that one side converges with the bottom electrode (separated by a dielectric layer). The top electrode is also compliant. As the voltage across the two electrodes increases, the force between them increases as well and the flexible beam will start to deform. Note that the force between the electrodes will be greatest at the convergence, or 'zipper' point where the two electrodes are tangential because that is the point at which d is smallest. As the actuation voltage increases, the zipper point moves down the length of the electrodes, bringing the tips together. This design increases the displacement and the analog operating range in comparison to the parallel plate capacitor [22]. The performance of these actuators can be enhanced by the addition of a dielectric liquid that has a higher ϵ and dielectric breakdown strength than air, and this has been applied to hydraulic pumps and ribbon actuators [25, 26].

3. Design

In this paper we present three potential designs for electrostatically actuated hinges. In each design the tip displacement of the zipper drives angular displacement of a flexural hinge through a mechanical transmission. The designs differ in their transmission geometry.

The linkage design approximates a four-bar linkage (figure 2(a)). The zipper tip, flexural hinge, and attachment point connecting the output linkage and zipper act like rotational joints while the elements connecting these points act like rigid beams. The sliding-surface design shares a similar resting profile to the linkage design, but the attachment point slides along the output linkage surface (figure 2(b)). This allows it to deflect farther under small voltages, but the friction causes the system to behave unpredictably. In both designs, the compliance of the hinge is increased by cutting 'windows' into the flexural layer.

The double zipper hinge increases the maximum torque by increasing the overall system stiffness and including zippers on both sides of the hinge (figure 2(c)). Because the bottom electrode extends across the hinge, we did not cut windows into the flexural layer. As a consequence, it has substantially lower angular displacement. As the zippers actuate, they push against each other horizontally, resulting in torque on the flexural hinge.

Each hinge is 20 mm wide, with 13 mm wide electrodes and 3.5 mm border of dielectric material on either side to prevent arcing. In the linkage and sliding-surface designs, the zipper is 52 mm long and 12 mm tall at its tip. The flexural hinge extends another 15 mm from the zipper and the output linkage is another 15 mm. The double-zipper design has a total electrode length (including both zippers) of 60 mm and is 4 mm tall at the center. The linkage and sliding-surface designs each weigh 1.5 g and the double-zipper weighs 1.9 g.

4. Fabrication

All hinges were designed to be fabricated with commercially available off-the-shelf tools and materials in a repeatable manner. Each electrode was composed of 50 μm thick 110 annealed copper sheet metal (Lyon Industries CUX-2). The dielectric layer between the electrodes was 50 μm thick polyimide film (Dupont). This layer was also used as a flexural hinge and output link due to its favorable elastic mechanical properties and convenient geometric location. The layers were adhered together with 50 μm polyimide tape with 38 μm silicone adhesive backing (Saint-Gobain CHR 2345-2). In the linkage design, the top electrode and transmission were bonded with glue (Locktite 4903) and the transmission and output were bonded with double-sided tape (3M Scotch).

The copper layers were cut with a fiber laser and the polyimide layers were cut with a CO_2 laser (PLS6MW, universal Laser Systems). The copper was held flat during cutting with a gel pack backing (WF-60-X4-A, Gel-Pak) to ensure a clean and even cut. Each layer was cut with an oversized boundary to accommodate two horizontally spaced

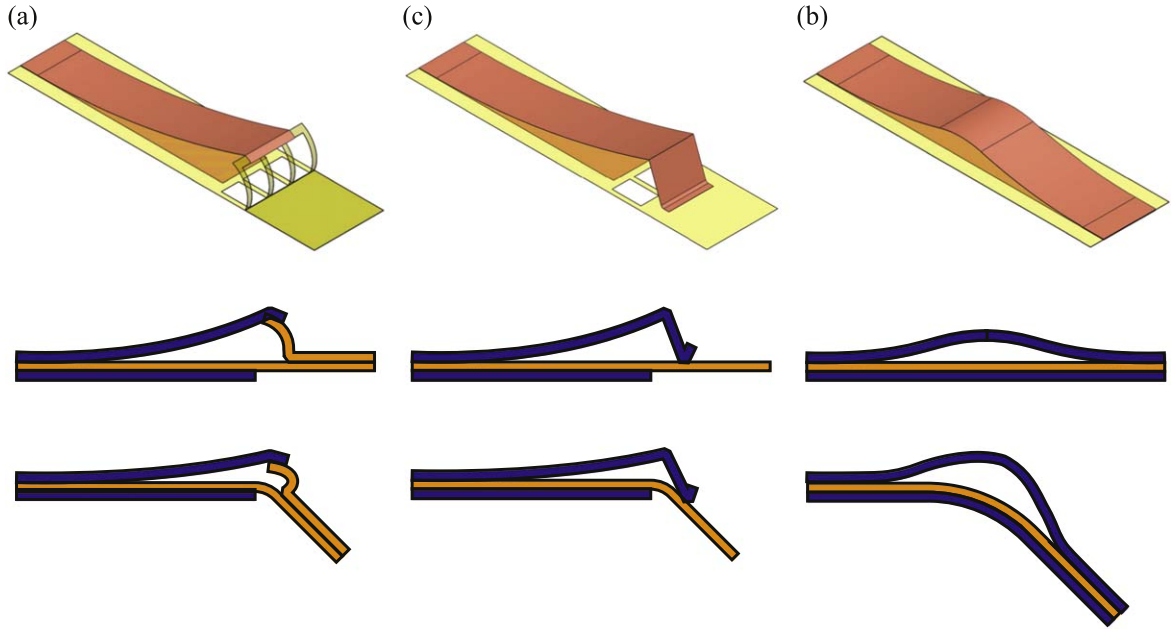

Figure 2. Three designs were developed and tested, each with a different transmission mechanism. (a) The linkage design. (b) The sliding-surface design. (c) The double-zipper design. An isometric drawing (top), unactuated side view (center), and actuated side view (bottom, with exaggerated displacement) are shown for each design.

alignment holes. Once the strips were cut and removed from the laser cutter, they were wiped clean and rolled flat.

First, the bottom electrode layer was laid on top of the dielectric layer, aligned on top of a base jig using dowel pins and alignment holes. A layer of 50 μm thick, 19 mm wide polyimide tape was rolled over the electrode, forming the hinge base. The base was then flipped and placed back on the base jig so that the polyimide tape was on bottom. A curved electrode-shaping jig was placed on top of dielectric layer, the upper electrode was laid on top of that, and the upper part of the electrode-shaping jig was installed, sandwiching the top electrode and fixing it along a specific curve. The entire jig assembly was clamped together and a 19 mm wide piece of polyimide tape was taped across the top electrode at the point where the two electrodes converge.

The jig assembly was placed in an oven at 200 °F. Although this is well below the annealing temperature of copper, we observed that this step improved the quality of the electrode curvature substantially. The assembly was removed and the excess copper and polyimide were trimmed, leaving 10 mm of each layer at the end for a circuit connection interface. An extra layer of polyimide tape was added around the dielectric layer to prevent unwanted electrostatic discharge.

Before operation, a small amount of dielectric oil (Envirotemp FR3) was applied to the electrodes where they connect. This addition was based on previous results demonstrating that dielectric liquid can substantially increase the performance of electrostatic zipper hinges [25, 26].

5. Modeling

A model of the electrostatic zipper hinge is based on Euler–Bernoulli beam theory, using an approach first established by Li *et al* [23] (figure 3). We start with the differential equation relating the beam deflection w with the force per unit length q distributed along a beam.

$$EI\frac{d^4w}{dx^4} = q(x). \tag{2}$$

In this case, the force is due to electrostatic attraction, and can be expressed as

$$q(x) = \frac{dF_a}{dx} = -\frac{\epsilon_l \epsilon_0 b V^2}{2\left[\left(\frac{\epsilon_l}{\epsilon_p}\right)d_p + y(x) + d_a\right]^2}, \tag{3}$$

where b is the electrode width, ϵ_0 is the vacuum permittivity, ϵ_l is the relative permittivity of the dielectric oil, d_p and ϵ_p are the thickness and relative permittivity of the polyimide insulator, y is the vertical space between the top electrode and polyimide layer, and d_a represents an additional space between the electrodes due to fabrication irregularities. Derivation of this equation can be found in [26].

The beam has a resting position c which can be expressed by a quadratic equation.

$$c(x) = \frac{\delta_0}{L_0^2}x^2 \qquad y(x) = c(x) + w(x), \tag{4}$$

where δ_0 is the vertical distance from the tip of the top electrode to the bottom of the flexible electrode in its resting state so that $\delta_0 = y(L_0)$ when $V = 0$, L_0 is the length of the bottom electrode, and x is the horizontal distance rightward starting at the left of the zipper. To solve this equation, we need to define four boundary conditions. At $x = 0$, the beam

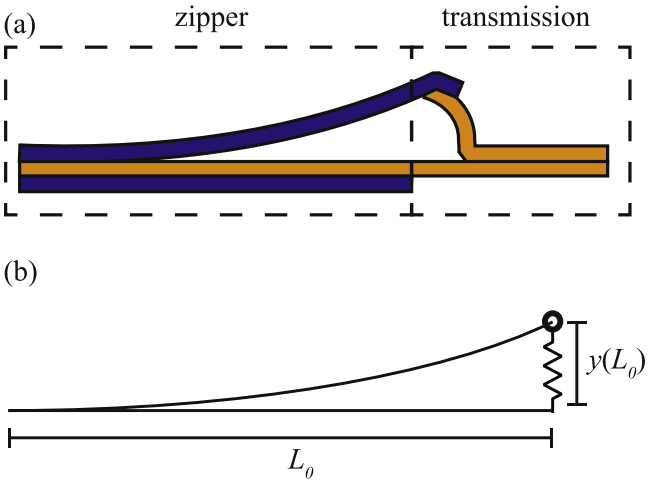

Figure 3. (a) The hinges can be treated as two components: the zipper drives a linear displacement at the zipper tip, and the transmission translates the linear motion into an angular displacement. (b) The zipper is modeled as an Euler–Bernoulli beam under a distributed load with a spring at its tip.

Table 1. Performance parameters of the hinges.

Design	Zipper tip stiffness k (N m^{-1})	Maximum angle θ_{max} (°)
Linkage	2.8	100
Sliding-surface	1.2	80
Double-zipper	170	90

position and slope are fixed, and at the tip ($x = L_0$), there is a negligible moment and a shear force F_{tip} due to the transmission.

$$w(0) = 0 \qquad w'(0) = 0 \qquad w''(L_0) = 0 \qquad w'''(L_0) = \frac{F_{tip}}{EI} \tag{5}$$

We model F_{tip} as an ideal spring $kw(L_0)$ and a gravity force F_g due to the transmission and output linkage, where k is a spring force dependent on the hinge design (table 1). For the linkage and sliding-surface designs, k was characterized experimentally by applying a point force to the zipper tip and measuring the force as a function of displacement. For the double-zipper design, k was fit using the data.

From this model, the zipper tip displacement $y(L_0)$ is calculated using a numerical boundary value problem solver. To relate the tip displacement with angular output, we assume a linear relationship.

$$\theta = \frac{\delta_0 - y}{\delta_0}\theta_{max}. \tag{6}$$

θ_{max} was determined experimentally for each hinge and represents complete pull-in of the zipper (table 1).

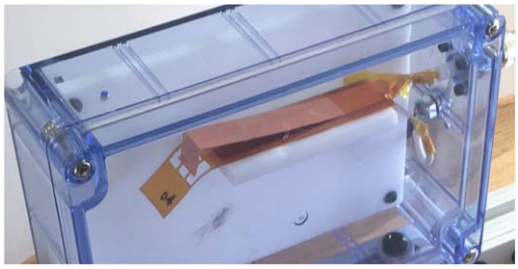

Figure 4. Experimental setup for measuring angular displacement.

Table 2. Step response characteristics for a single sample of each design in response to a 5 kV input. Mean ± standard deviation, $n = 3$.

Design	Displacement (°)	Rise time (ms)	Input energy (J)
Linkage	46.6 ± 1.8	69 ± 6	5.85 ± 0.51
Sliding-surface	30.5 ± 0.3	68 ± 5	6.30 ± 0.19
Double-zipper	5.4 ± 0.3	117 ± 2	5.85 ± 0.66

6. Experiments and results

6.1. Step response

We applied a 5 kV step input for two seconds to observe the displacement and speed of each hinge. For each experiment, we placed the sample inside a plastic enclosure and fixed the bottom electrode to an acrylic base with double sided tape (figure 4). We recorded the actuator with a high-speed camera at 960 fps. We analyzed the video with a MATLAB script to calculate the hinge angle at each frame of the test. We used a Matsusada Precision AMT-5B20 5 kV DC voltage amplifier to generate the high voltage signals and a BK Precision 2190E 2-channel oscilloscope to measure the current from the power supply. We controlled the high-voltage supply with an Arduino Uno generating 0–5 V analog signal. To sync the voltage and current data collected from the oscilloscope to the hinge angle calculated from the high-speed camera, we generated a syncing pulse from the Arduino that triggered the oscilloscope to start recording and turned on an LED in the camera's frame of view, allowing us to correlate these time points in post-processing.

For each design, we tested a single sample in three separate trials, manually resetting the hinge between inputs. We calculated the final angle and rise time (up to first peak) of each test and measured the current drawn over time to calculate the total electrical energy input (table 2). We plotted each step response as a function of time (figure 5).

Each design had some resting angle due to gravity between 20° and 45°. The hinges were designed to be compliant to maximize displacement, but this made them susceptible to body forces. The linkage and sliding-surface designs both reached their maximum angular displacement,

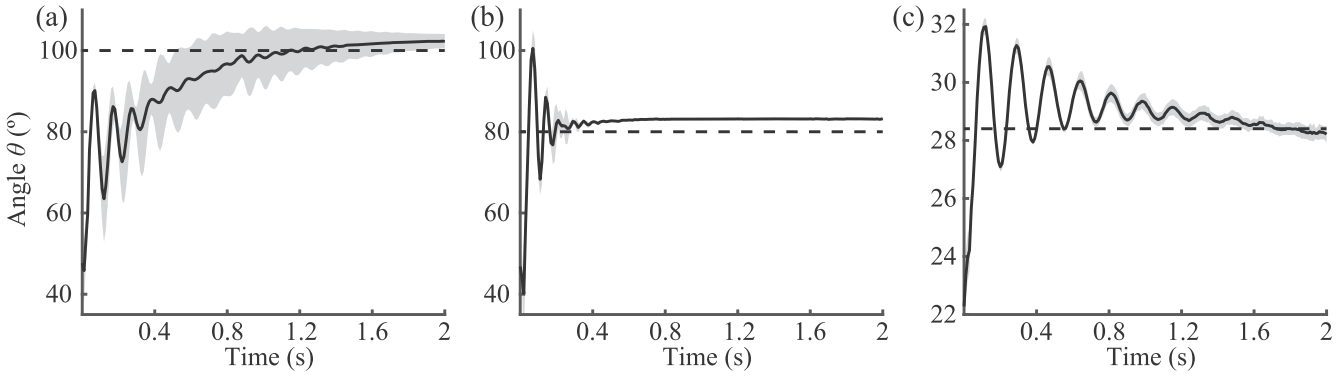

Figure 5. The absolute angle as a function of time in response to a 5 kV step input for one sample of (a) the linkage design, (b) the sliding-surface design, and (c) the double-zipper design. The dashed line indicates model-predicted steady-state response. Shaded regions indicate standard deviation, $N = 3$.

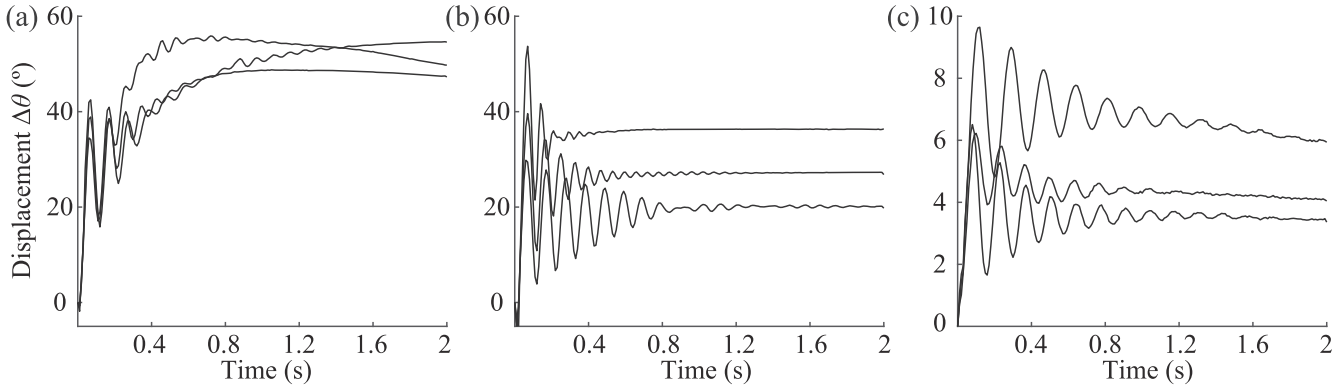

Figure 6. The angular displacement as a function of time in response to a 5 kV step input for three samples of (a) the linkage design, (b) the sliding-surface design, and (c) the double-zipper design. Each line represents the mean angle from three different trials.

while the double-zipper hinge displacement was substantially below the maximum.

The hinges all showed satisfactory repeatability ($\leqslant$5%) between trials. They also showed fast response times of approximately 50 ms for the linkage and sliding-surface designs and 120 ms for the double-zipper design.

We then tested two more samples of each design (three samples total) in three trials and compared their displacement (figure 6). We observed some variation between samples but also noted that each design exhibited certain characteristics common between samples. The linkage design was the most consistent across samples and exhibited higher order dynamics, with a slow overdamped response in addition to the fast underdamped one. The sliding surface design exhibited a large overshoot and substantial variability in settling time and max displacement between samples, likely due to the friction forces that dominate the system dynamics. The double-zipper also had substantial variability in displacement, but had a consistent natural frequency and settling time across samples.

Each design exhibited some drift over multiple step inputs, which is why the previous experiments were all performed after manually resetting the hinges. To characterize this drift, we performed 10 sequential step inputs to a single sample of each design without manual resetting. After each step input, the voltage was reset to 0 and the hinge was allowed to fully relax. The sliding-surface design always held its maximum angular displacement, and so could not be actuated repeatedly without manually resetting. For the linkage and double-zipper designs, we observed that although there was an initial change in the resting position after the first few steps, subsequent step inputs did not cause the resting position to change further (figure 7). We also observed that the shape of the input response changed slightly with successive steps, particularly in the linkage design.

6.2. Torque and energy characterization

We characterized the torque of each design with blocked-torque measurements. We tested three samples of each design with step inputs of increasingly higher amplitudes up to 5 kV (figure 8). The linkage and sliding-surface designs showed similar torque-voltage profiles, which aligns with their similar geometries in the blocked state. The double-zipper demonstrated substantially larger torques, and we expect this is due to a combination of the double-actuator architecture and the higher transmission stiffness. From these measurements and their step response we estimated their stroke energy $E_s \approx \theta_{\max} \tau_{\max} / 2$ (table 3). Although we expect that the torque as a function of angular displacement is nonlinear, we can use this value to gain some insight into their stroke energy.

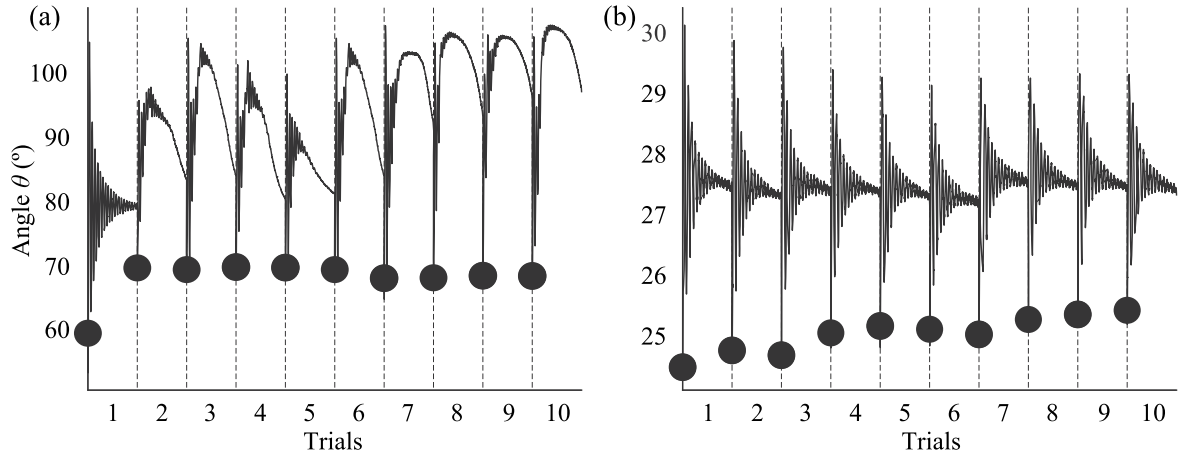

Figure 7. Angle of (a) the linkage design and (b) the double-zipper design in response to 10 sequential step inputs without manual reset of hinge's initial angle. Dots indicate the resting angle between each step and dashed lines separate each step.

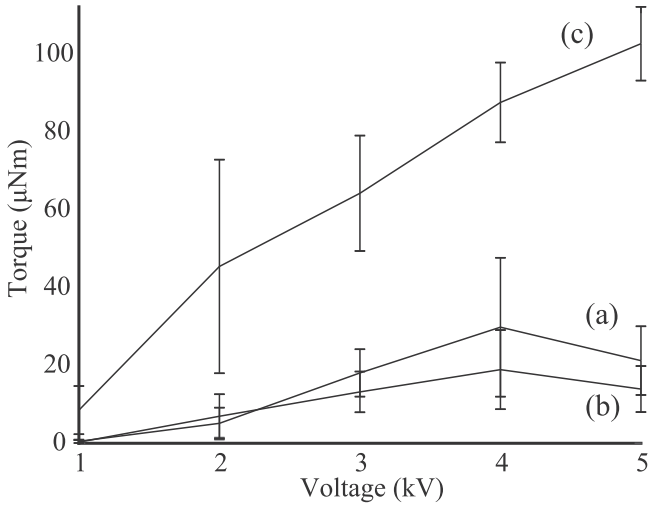

Figure 8. Blocked torque of the (a) linkage, (b) sliding-surface, and (c) double-zipper designs. Error bars indicate standard deviation, $N = 3$.

6.3. Ramp response

To observe the linearity and hysteresis of the hinges, we subjected three samples of each design to a triangle-wave voltage input, consisting of three ramps with increasing peak voltages of 1, 3, and 5 kV at a rate of 200 V s^{-1}. We observed the output angle using the same process and equipment as for the step response experiments, except that we used an Samsung Galaxy S7 camera at 240 fps to record displacement.

The linkage design showed relatively continuous displacement in response to the initial voltage increase (figures 9(a)–(b)). However, it exhibited an interesting response to decreasing voltage, in which the displacement would initially decrease, and then increase as the voltage approached zero, resulting in a U-shaped voltage-displacement curve on subsequent ramps. This behavior appeared regularly across all samples and trials. The actuator reached its maximum displacement at approximately 2.5 kV.

The sliding surface design showed discrete jumps as well as bistable pull-in behavior (after which the system remained

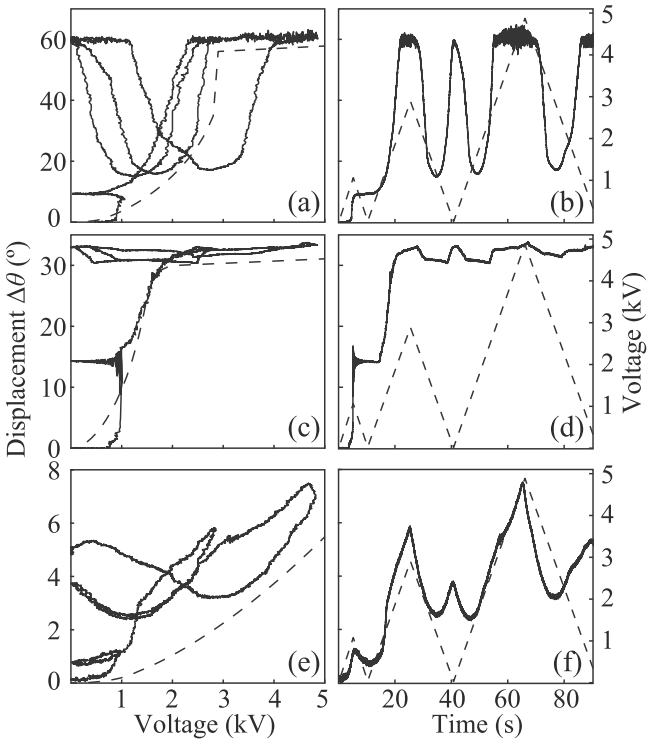

Figure 9. Angular displacement of the hinges in response to a triangle-wave signal with increasing peaks (1, 3, 5 kV). (a)–(b) Linkage design as a function of (a) voltage and (b) time. (c)–(d) Sliding-surface design as a function of (c) voltage and (d) time. (e)–(f) Double-zipper design as a function of (e) voltage and (f) time. Each plot is a single trial. Dashed lines represent the modeled displacement (a), (c), (e) and voltage (b), (d), (f).

Table 3. Blocked torque and estimated energy characteristics of the electrostatic zipper hinges at 5 kV. Mean ± standard deviation, $N = 3$.

Design	Torque (μN-m)	Stroke Energy (μJ)
Linkage	21.2 ± 8.8	8.6
Sliding-surface	13.9 ± 5.9	3.7
Double-zipper	102.7 ± 9.5	4.8

at a maximum displacement) under voltages less than 1 kV, substantially less than the other designs (figures 9(c)–(d)). Once displaced, the actuator did not relax. This is likely due to the dominance of friction in the system dynamics, which makes the system nonlinear and highly hysteretic.

The double-zipper design also showed hysteresis, including the increase in displacement as the voltage returned to zero (figures 9(e)–(f)). However, it was less pronounced than in the other designs, and the hinge demonstrated analog behavior up to 5 kV.

7. Discussion

The results demonstrated the performance of electrostatically driven self-folding hinges and revealed differences between the designs. The linkage design showed a reasonable compromise between displacement and torque, making it the most promising candidate for continuous and controlled actuation. The double-zipper hinge had the least displacement but the highest torque. The sliding surface design showed the least repeatability and greatest hysteresis, but it did demonstrate the largest displacement in response to sub-kilovolt inputs.

These results indicate how each design is suited for different applications. the linkage design has a large continuous (but nonlinear) range over $\approx 60^{\circ}$ and is reversible, making it best suited for repeated and controllable actuation. In contrast, the sliding surface design would not be easy to control but does have large displacement at low voltages, so it would be better suited for discrete transformations such as flat-to-folded self-assembly. The double-zipper design has the highest torque and stroke energy, making it appropriate for the actuation of heavier structures, but only in applications where the angle needs to be adjusted within a few degrees. It could also be distributed along flexible surfaces to adjust tension, dynamically straightening thin surfaces. In all designs, the biggest challenge to future applications is in the limited torque and low stiffness of the actuators, limiting their effectiveness under gravity or other substantial body forces. While our torque results correspond to blocked tip forces on the order of hundreds of millinewtons, other work into zipper hinges have generated forces up to hundreds of newtons [26], so future work may be able to substantially improve the torque outputs.

Our proposed model helped us understand the differences between the three designs but did not capture their complete behavior. In particular, it did not predict the observed hysteresis. We believe that this may be due to a combination of plastic deformation and viscous behavior from the dielectric oil. The increase in displacement during the gradual decrease in voltage was unexpected and may be due to space charge accumulation in the polyimide layer [27, 28]. Further experiments must be conducted to determine its cause.

Variations between different samples indicate that our fabrication process is not repeatable enough for precise applications. This is supported by the model, which suggests that small changes in initial position will result in large differences in angular displacement. A few of the challenges include the application of a precise curve to the upper electrode, avoiding microscale dents and creases in the copper, and precise position of the polyimide dielectric layers. Further research can look into high-temperature annealing to remove prestress from the electrodes, better layup jigs for precise layer alignment, and alternative bending methods for patterning the upper electrode curvature.

If these challenges can be addressed, there are several interesting avenues for future research. One possibility is to use the capacitance of the zipper as a sensor to measure the angular displacement. Previous angular sensors in self-folding hinges have had challenges with accuracy [29] and miniaturization [30], so a structure with inherent actuation and sensing would be valuable for controlled transformation. We could also use our model to optimize the resting curvature of the electrode $c(x)$ to maximize precision, power, or even tailor it to create arbitrary voltage-displacement curves. If the fabrication process could be minimized, we expect that, like traditional electrostatics, this design would be well-suited to the sub-millimeter scale level. Finally, connecting multiple actuators in series or parallel could result in interesting and highly adaptive structures.

In summary, the electrostatic zipper design is a promising and flexible approach to fast and repeatable self-folding. These mechanisms have the potential for precise and controllable actuation of complex planar structures.

Acknowledgments

This work was funded by Northeastern University.

ORCID iDs

Samuel M Felton https://orcid.org/0000-0002-0545-9617

References

[1] Ma X, Vogtmann D and Bergbreiter S 2016 Dynamics and scaling of magnetically folding multi-material structures *2016 IEEE Int. Conf. on Robotics and Automation (ICRA)* (Piscataway, NJ : IEEE) pp 1899–906

[2] Rogers J, Huang Y, Schmidt O G and Gracias D H 2016 Origami mems and nems *MRS Bull.* **41** 123–9

[3] Filipov E T, Tachi T and Paulino G H 2015 Origami tubes assembled into stiff, yet reconfigurable structures and metamaterials *Proc. Natl Acad. Sci.* **112** 12321–6

[4] Overvelde J T B, De Jong T A, Shevchenko Y, Becerra S A, Whitesides G M, Weaver J C, Hoberman C and Bertoldi K 2016 A three-dimensional actuated origami-inspired transformable metamaterial with multiple degrees of freedom *Nat. Commun.* **7** 10929

[5] Felton S, Tolley M, Demaine E, Rus D and Wood R 2014 A method for building self-folding machines *Science* **345** 644–6

[6] Dufour L, Owen K, Mintchev S and Floreano D 2016 A drone with insect-inspired folding wings *2016 IEEE/RSJ Int. Conf. on Intelligent Robots and Systems (IROS)* (Piscataway, NJ : IEEE) pp 1576–81

[7] Kim S-J, Lee D-Y, Jung G-P and Cho K-J 2018 An origami-inspired, self-locking robotic arm that can be folded flat *Sci. Robot.* **3** eaar2915
[8] Miura K 1985 Method of packaging and deployment of large membranes in space *Inst. Space Astronaut. Sci. Rep.* **618** 1–9
[9] Zirbel S A, Lang R J, Thomson M W, Sigel D A, Walkemeyer P E, Trease B P, Magleby S P and Howell L L 2013 Accommodating thickness in origami-based deployable arrays *J. Mech. Des.* **135** 111005
[10] Paik J K and Wood R J 2012 A bidirectional shape memory alloy folding actuator *Smart Mater. Struct.* **21** 065013
[11] Liu Y, Boyles J K, Genzer J and Dickey M D 2012 Self-folding of polymer sheets using local light absorption *Soft Matter* **8** 1764–9
[12] Guan J, He H, Hansford D J and Lee L J 2005 Self-folding of three-dimensional hydrogel microstructures *J. Phys. Chem.* B **109** 23134–7
[13] Liu C and Felton S M 2017 A self-folding robot arm for load-bearing operations *2017 IEEE/RSJ Int. Conf.on Intelligent Robots and Systems (IROS)* (Piscataway, NJ : IEEE) pp 1979–86
[14] Na J-H, Evans A A, Bae J, Chiappelli M C, Santangelo C D, Lang R J, Hull T C and Hayward R C 2015 Programming reversibly self-folding origami with micropatterned photo-crosslinkable polymer trilayers *Adv. Mater.* **27** 79–85
[15] Tolley M T, Felton S M, Miyashita S, Aukes D, Rus D and Wood R J 2014 Self-folding origami: shape memory composites activated by uniform heating *Smart Mater. Struct.* **23** 094006
[16] Felton S M, Becker K P, Aukes D M and Wood R J 2015 Self-folding with shape memory composites at the millimeter scale *J. Micromech. Microeng.* **25** 085004
[17] Reddy S Y, Frank J D, Iatauro M J, Boyce M E, Kürklü E, Ai-Chang M and Jónsson A K 2011 Planning solar array operations on the international space station *ACM Trans. Intell. Syst. Technol.* **2** 41
[18] Jin Q-B, Huang J and Fan J-Y 2015 Motion analysis and trajectory planning of solar tracking of a class of space solar power station *Sol. Energy* **122** 239–48
[19] Shintake J, Rosset S, Schubert B, Floreano D and Shea H 2016 Versatile soft grippers with intrinsic electroadhesion based on multifunctional polymer actuators *Adv. Mater.* **28** 231–8
[20] Judy J W 2001 Microelectromechanical systems (mems): fabrication, design and applications *Smart Mater. Struct.* **10** 1115
[21] Hung E S and Senturia S D 1999 Extending the travel range of analog-tuned electrostatic actuators *J. Microelectromech. Syst.* **8** 497–505
[22] Brenner M P, Lang J H, Li J and Slocum A H 2004 Optimum design of an electrostatic zipper actuator *NSTI Nanotech 2004* **2** 371–4
[23] Li J *et al* 2004 Electrostatic zipping actuators and their applications to MEMS *PhD Thesis* Massachusetts Institute of Technology
[24] Chen A S, Zhu H, Li Y, Hu L and Bergbreiter S 2014 A paper-based electrostatic zipper actuator for printable robots *2014 IEEE Int. Conf. on Robotics and Automation (ICRA)* (Piscataway, NJ : IEEE) pp 5038–43
[25] Kellaris N, Venkata V G, Smith G M, Mitchell S K and Keplinger C 2018 Peano-hasel actuators: muscle-mimetic, electrohydraulic transducers that linearly contract on activation *Sci. Robot.* **3** eaar3276
[26] Taghavi M, Helps T and Rossiter J 2018 Electro-ribbon actuators and electro-origami robots *Sci. Robot.* **3** eaau9795
[27] Yao T-J, Walsh K and Tai Y-C 2002 Dielectric charging effects on parylene electrostatic actuators *Technical Digest. MEMS 2002 IEEE Int. Conf. Fifteenth IEEE Int. Conf. on Micro Electro Mechanical Systems (Cat. No. 02CH37266)* (Piscataway, NJ : IEEE) pp 614–7
[28] Zhou L R, Wu G N, Gao B, Zhou K, Liu J, Cao K J and Zhou L J 2009 Study on charge transport mechanism and space charge characteristics of polyimide films *IEEE Trans. Dielectr. Electr. Insul.* **16** 1143–9
[29] Sun X, Felton S M, Wood R J and Kim S 2015 Printing angle sensors for foldable robots *2015 IEEE/RSJ Int. Conf. on Intelligent Robots and Systems (IROS)* (Piscataway, NJ : IEEE) pp 1725–31
[30] Nisser M E W, Felton S M, Tolley M T, Rubenstein M and Wood R J 2016 Feedback-controlled self-folding of autonomous robot collectives *2016 IEEE/RSJ Int. Conf. on Intelligent Robots and Systems (IROS)* (Piscataway, NJ : IEEE) pp 1254–61